HEAT LOSSES IN APPLIED SMOULDERING SYSTEMS: SENSITIVITY ANALYSIS VIA ANALYTICAL MODELLING

Tarek L. Rashwan [a, b], José L. Torero [c], Jason I. Gerhard [a*]

[a] Department of Civil and Environmental Engineering, The University of Western Ontario, London, Ontario N6A 5B9, Canada

[b] Department of Civil Engineering, Lassonde School of Engineering, York University, Toronto, Ontario, M3J 1P3, Canada [1]

[c] Department of Civil, Environmental and Geomatic Engineering, University College London, London, WC1E 6BT, UK

* Corresponding author at: Department of Civil and Environmental Engineering, The University of Western Ontario, Spencer Engineering Building, Rm. 3029, London, Ontario N6A 5B9, Canada. Tel.: +1 (519) 661 4154; fax: +1 (519) 661 3942. E-mail address: jgerhard@uwo.ca (J. I. Gerhard).

[1] Present address.

One file containing supplementary materials is available.

Abstract: As smouldering-based systems gain popularity for a variety of energy conversion purposes, there is a strong interest in optimizing the reactor design to support robust smouldering. Heat losses play a critical role in the energy balance of smouldering system, and therefore have strong implications toward understanding propagation limits and reactor design. Heat losses in a forward smouldering system were approximated by adapting the analytical model from Kuznetsov (1996), originally developed for unsteady local thermal non-equilibrium heat transfer in a porous cylinder, to simulate the cooling zone trailing the smouldering front. The analytical model was adapted to a smouldering system by solving on a domain that lengthens as the cooling zone expands at the rate of the smouldering velocity. The results are incorporated into a global energy balance on the smouldering system, thereby providing an inexpensive and rapid method to estimate the system energy efficiency. Confidence in the analytical model was provided by demonstrating its predictions compare well with existing experimental and numerical estimates of heat losses from similar smouldering systems. The model was then used to quantify the sensitivity of the heat losses to two key reactor design parameters: radius and insulation quality. The system energy efficiency was shown to be highly sensitive to improved insulation and increased radius up to ~0.1 m (i.e., laboratory-sized reactors). However, this sensitivity diminished with size. Beyond 0.4 m radius, the predicted system energy efficiency was high (~85-95%) and relatively insensitive to reactor radius and insulation quality. Therefore, commercial, batch treatment smouldering reactors do not need to be larger than 0.4 m in radius to protect against heat losses and maximize their energy efficiency. This threshold design radius is considerably less than used in current reactors and therefore can provide valuable cost savings.

Keywords: Smoldering combustion; Local thermal non-equilibrium; Energy balance; Heat losses; Porous media; Process scale-up.

Nomenclature

Abbreviations

DT	Dimensionless Time
IPM	Inert Porous Media
LTNE	Local thermal non-equilibrium

Latin Letters

a_{sg}	Specific surface area, m^{-1}
b_n	Positive root from transcendental equation (1), -
C_p	Specific heat capacity, J kg^{-1} K^{-1}
d_p	Particle diameter, m
E	Energy, J
$\dot{E}$	Energy rate, J s^{-1}
fr_{CO}	Fraction of carbon oxidized to carbon monoxide
h	Heat transfer coefficient, W m^{-2} K^{-1}
h_{sg}	Interfacial heat transfer coefficient, W m^{-2} K^{-1}
H	Modified heat transfer coefficient, m^{-1}
J_a	the Bessel function of the first kind
k	Thermal conductivity, W m^{-1} K^{-1}
l	Length, m
L	Dimensionless length, -
m/m	Mass fraction, -
$\dot{m}''$	Mass flux, kg m^{-2} s^{-1}
Nu	Nusselt Number, -
Pr	Prandtl number, -
Re	Reynold's number, -
r_o	Outer radius, m
R	Dimensionless outer radius, -
t_c	Characteristic time, s
T_{peak}	Maximum temperature, K
T_{amb}	Ambient temperature, K
u_g	Darcy flux, m s^{-1}
v_{oxid}	Smouldering velocity, m s^{-1}
v_{cool}	Cooling velocity, m s^{-1}
W	Volumetric mass loss, kg m^{-3} s^{-1}
x_c	Characteristic distance, m

Greek Symbols

α	Dimensionless modified heat transfer coefficient, -

γ_m	Positive root from a transcendental equation (2), -
δ	Small dimensionless parameter, -
μ	Dynamic viscosity, Pa·s
ξ	Dimensionless distance, -
ρ	Density, kg m^{-3}
σ	Stephan Boltzmann constant, W m^{-2} K^{-4}
τ	Dimensionless time, -
ϕ	Porosity, -
$\Delta\xi$	Difference between dimensionless distances, -
$\Delta\theta$	Dimensionless difference between air and solid temperatures, -
ΔH_{oxid}	Heat of smouldering, MJ kg^{-1}
Λ	Constant, -

Subscripts

0	Initial
amb	Ambient
app	Approximate
c	Characteristic
$cool$	Cooling
eff	Effective
f	Final
g	Gas/air
in	Into control volume
ins	Insulation
j	Discretized position
J	Final discretized position
$loss$	Lost from control volume
net	Net stored
out	Out of control volume
$oxid$	Oxidation
pyr	Pyrolysis
r	Radial
s	Solid/sand
x	Axial

1. Introduction

Smouldering combustion research has traditionally focused on hazards in combustible porous materials (e.g., polyurethane foam, biomass), including within home furniture, spacecrafts, coal mines, and peatland fires [1-4]. However, smouldering (sometimes called filtration combustion [5-8]) is also being used as an engineering tool across various disciplines to address a wide range of challenges. It is clear from applications such as brownfield site remediation [9-13], energy conversion [5, 14], wastewater sludge treatment [15, 16], waste processing and resource recovery [6, 17], and sanitation in the developing world [18], that smouldering is emerging as a simple, economical, and robust technology. Many smouldering applications are implemented with large scale commercial systems, e.g., batch reactors for treating stockpiled hazardous waste [9-11, 19]. These sizes are increasing as the technology develops, where some systems can exhibit an effective radius of 6 m and treat upwards of 34 tonnes of material per day [20]. It is assumed that heat losses at this scale negligibly impact the system's energy balance, although this has never been studied and the system design has neglected such considerations. Meanwhile, smouldering research has almost exclusively been performed at the laboratory scale where heat losses are high. No method exists for evaluating the sensitivity of heat losses to radius or other key design parameters and there exists no strategy for extrapolating from the laboratory scale to the field scale in these systems.

Smouldering is a flameless form of combustion driven by gaseous oxygen directly reacting with the surface of a condensed phase fuel [21-23]. In many smouldering applications, the fuel is embedded in a fixed bed of inert porous media (IPM) such as

sand or soil [15, 20, 23] and air is continuously injected at the inlet to support the reaction. The smouldering reaction, converting fuel into primarily carbon dioxide and heat, propagates through the fuel/inert bed as a reaction wave. The complex interaction of heat and mass transfer with chemical processes typically results in the propagation of a self-sustaining smouldering reaction [23]. Self-sustaining in this context means that, after an initial ignition event, the reaction propagates without additional external energy input; this characteristic is one of the key reasons that smouldering applications rank very highly in energy and cost efficiency [20].

The self-sustaining smouldering wave exhibits distinct zones, each characterized by its dominant chemical and physical processes [21, 23-25]. Figure 1 highlights three zones that dominate many applied smouldering systems: *inert heating zone*, *reaction zone*, and *cooling zone* [23]. The *inert heating zone,* characterized by endothermic physical processes, exhibits preheating of the fuel bed driven by the heat released by smouldering. Here, volatile compounds (including water) change phase and are convected forward with the air flow. Upstream is the *reaction zone,* characterized by the endothermic pyrolysis and exothermic oxidative reactions that drive smouldering propagation. Many different reactions may compete in this zone [23, 25], however, pyrolysis generally precedes oxidation [21, 26]. Further upstream is the *cooling zone*, which is subdivided into *Region 1* (strongly influenced by axial convection-conduction) and *Region 2* (strongly influenced by radial conduction and perimeter heat losses). Like the inert heating zone, the cooling zone is devoid of chemical reactions and instead exhibits heat exchange between the remaining inert material (solid phase) and air (gas phase). In other words, heat transfer here fundamentally results from local thermal non-equilibrium (LTNE).

The propagation direction and velocities of the interfaces between these zones are critical to defining the smouldering scenario. Figure 1 illustrates that the smouldering front coincides with the sharpest temperature increase near the beginning of the reaction zone and travels with the smouldering velocity (v_{oxid}). The cooling front coincides with the sharpest temperature decrease near the end of the cooling zone and travels with cooling velocity (v_{cool}). The end of the cooling zone lags slightly behind the cooling front because of conduction and this distance grows with time (t) as $\sqrt{t}/2$ [7, 8]. Figure 1 illustrates a "forward smouldering" scenario, defined as when the smouldering reaction and the oxidizer (air) are travelling in the same direction [21, 26]. It also illustrates a "reaction-leading" scenario, where $v_{oxid} > v_{cool}$ [8]. Forward, reaction-leading scenarios dominate applied smouldering systems (e.g., [9-11, 15, 19, 20, 23, 27]).

Figure 1 highlights that, in applied smouldering systems, the cooling zone is often much thicker (O(0.1-1 m)) than the other zones, especially the reaction zone (O(0.001-0.01 m)) [28-31]. Therefore, the cooling zone-reaction zone interface is often very close to the smouldering front. Moreover, the cooling zone expands with time since $v_{oxid} > v_{cool}$ (while the expansion will eventually stop, that occurs at batch reactor lengths beyond practical limits). As a result, energy released from smouldering accumulates in the IPM within the cooling zone, resulting in high temperatures between the cooling and smouldering fronts. These cooling zone characteristics – long and hot – mean that it is the zone most susceptible to perimeter heat losses. Zanoni et al., [28, 32] demonstrated that >90-95% of the heat losses from a laboratory-sized reactor were related to perimeter losses from the cooling zone. Therefore, the cooling zone is the primary zone of interest in studying heat losses from applied smouldering systems.

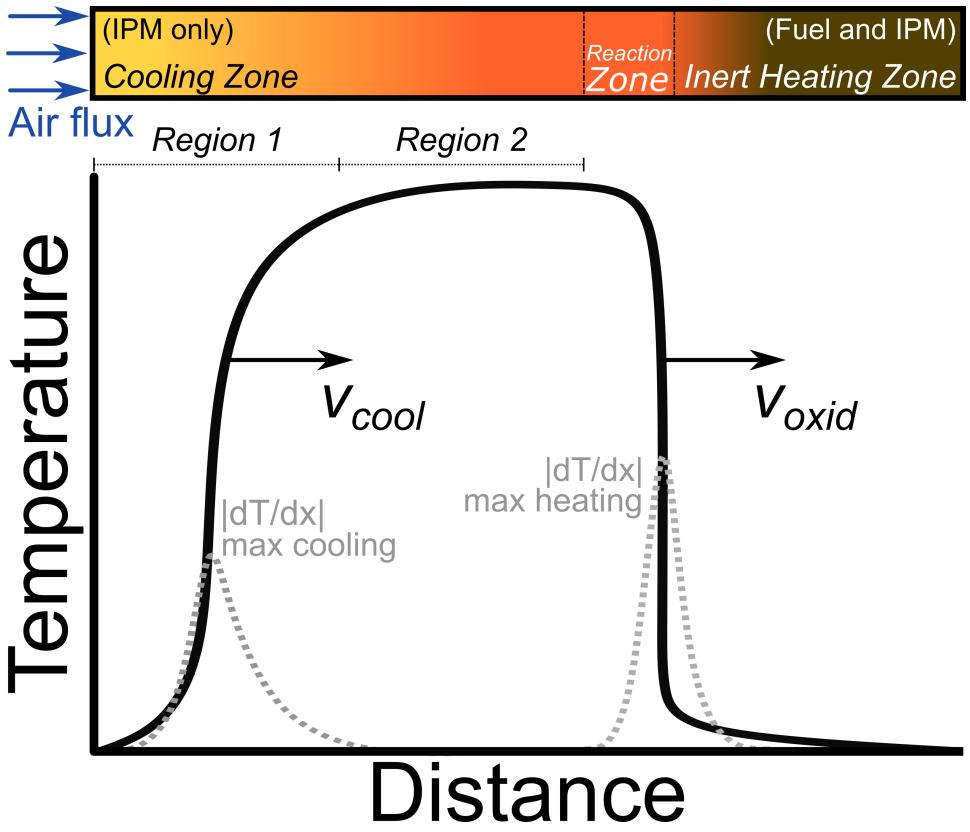

Fig. 1. Conceptual model of the centreline characteristics of a forward smouldering reactor that is reaction-leading, where the *Inert Heating Zone*, *Reaction Zone*, and *Cooling Zone* (further divided into *Region 1* and *Region 2*) are highlighted for discussion. These zones are bounded approximately by the velocities of the smouldering front (v_{oxid}) and the cooling front (v_{cool}). The temperature distribution across distance is presented and overlain with the approximate $|dT/dx|$ profile (dashed grey line) to show how the zone boundaries correspond to the temperature profile. Here, propagation is assumed fuel-limited, so fuel within the inert porous medium (IPM) is completely consumed in the reaction zone, and only IPM is present in the cooling zone.

Engineered smouldering systems are self-sustaining as long as they support a net positive energy balance [23, 32]. The key terms governing the global energy balance over a smouldering system are [28, 32]:

$$\dot{E}_{net}(t) = \dot{E}_{in}(t) + \dot{E}_{oxid}(t) - \dot{E}_{pyr}(t) - \dot{E}_{loss}(t) - \dot{E}_{out}(t) \quad (1)$$

where $\dot{E}_{net}$ is the net rate of energy production; $\dot{E}_{in}$ and $\dot{E}_{out}$ are the rates of energy added into the system for ignition and lost from convection out of the system when smouldering propagates to the end of the fuel bed, respectively; $\dot{E}_{loss}$ is rate of energy lost to the environment as perimeter heat losses; $\dot{E}_{oxid}$ and $\dot{E}_{pyr}$ are the rates of energy released from exothermic chemical reactions and consumed by endothermic chemical reactions, respectively. $\dot{E}_{in}$ and $\dot{E}_{out}$ are boundary effects and can be neglected when smouldering propagates throughout much of the system. Furthermore, $\dot{E}_{pyr}$ is often small in applied smouldering that is robust (i.e., far from extinction) [28, 32]. Therefore, $\dot{E}_{net}$ is dominated by $\dot{E}_{oxid}$ on the positive side, a function of injected air flow and fuel type and concentration, and by $\dot{E}_{loss}$ on the negative side, a function of the cooling zone characteristics including length, temperature, system scale, and insulation [28]. As $\dot{E}_{oxid}$ increases and $\dot{E}_{loss}$ decreases, engineered smouldering systems become more robust and generate more excess energy that can be captured and used. Two example smouldering systems, and the use of Eq. (1) to highlight cooling zone characteristics, is provided in the Supplementary Materials, Section S1.

Of the design parameters that control heat loss, reactor radius and insulation quality are expected to be dominant. It seems intuitive that increasing the radius of a smouldering reactor should reduce the fraction of energy lost, since energy generation is a function of a reactor's volume ($\sim r_o^2$) while heat losses are a function of its surface area ($\sim r_o$). And while this relationship has not been modelled or explored in detail, the sparse data available supports this conclusion. Several studies suggest that approximately 30-50% of the energy generated by smouldering within insulated laboratory reactors is lost through the walls [28, 30-32]. Rashwan et al., [33], through highly instrumented

experiments, showed that approximately 35% of the energy was lost radially in a reactor with r = 0.08 m compared to 14% with r = 0.30 m. Large scale smouldering applications have further suggested indirectly that increasing scale corresponds to more robust smouldering scenarios [17, 27, 34]. While these few studies are supportive, no study has evaluated heat loss sensitivity to the key design parameters of radius and insulation.

To achieve this, a model is needed to simulate the energy balance in the system. The choice of model depends, in part, on the key system behaviour. As articulated above, commercial smouldering reactors invariably exhibit expanding cooling zones [9-11, 19]. This represents early time, dynamic heat losses during smouldering propagation. In contrast, late time, nearly steady-state cooling zones, which would occur theoretically in very tall reactors, is of little practical value (a definition and thorough discussion of the transition between these two regimes is provided in the Supplementary Materials, Section S1). Therefore, the temporal and spatial dependencies are critical to this problem and not easily captured with a scale analysis. Meanwhile, a numerical two-dimensional model is computationally expensive. Thus, an analytical model is ideal for identifying the governing physics and rapidly and inexpensively developing a quantifiable description of heat losses.

Kuznetsov [35, 36] reviewed the development of analytical solutions for LTNE transient heat transfer in porous media. Many of these solutions follow the Schumann [37] model, which simplifies the problem by neglecting conduction in the solid and fluid phases. The solution proposed by Kuznetsov [35] accounts for the nonlinearity imposed by LTNE through a perturbation analysis, thereby delivering an analytical description of the temperatures in two phases throughout space and time. Kuznetsov [38] then extended

the same perturbation technique from [35] to obtain a solution for two-dimensional unsteady heat transfer in an IPM reactor. Though Kuznetsov's model was unrelated to smouldering, it is highly suitable to analyze the (reaction-less) LTNE heat transfer within the cooling zone for an applied smouldering system (Fig. 1).

This paper provides a method for systematically quantifying the relationship between heat losses and key system parameters in applied smouldering reactors. This was accomplished by adapting the analytical solution for LTNE, two-dimensional radial, unsteady heat transfer from Kuznetsov [38] to a growing cooling zone behind a propagating smouldering front. The model was then compared to published data to develop confidence in its predictions. Furthermore, the model was employed to quantify the sensitivity of heat losses to reactor radius and insulation quality. In all cases, a global energy balance approach was used, where heat losses were compared with the energy added into the system by smouldering to estimate the system energy efficiency. While useful for smouldering systems, this insight is also valuable to other packed bed reactors e.g., for pyrolysis, gasification, or energy storage purposes [5, 39, 40]. Overall, this work provides novel and important insights into the role of system scale in reducing heat losses, allowing for designers to minimize cost and maximize the benefit from smouldering systems, such as energy recovery.

2. Methodology

2.1. Model Domain and Formulation

Based on the conceptual model in Fig. 1, Fig. 2(a) presents a sketch of a smouldering reactor and Fig. 2(b) shows the two-dimensional analytical model domain for solving heat losses from a reaction-leading, forward smouldering system in a reactor of radius r_o. As discussed earlier, the cooling zone alone was targeted for the analysis. Therefore, the model domain considered cooling of the fuel-free IPM with a fixed origin corresponding to the heater (igniter) position in many applied forward smouldering systems, e.g., [29, 41-43]. Fig. 2(b) identifies the relevant boundary and initial conditions. In this analysis, the cooling zone was assumed to start at the peak smouldering temperature, T_{peak}, and then was cooled by both forced air at ambient temperature, T_{amb}, and radial heat losses through the reactor insulation. This analysis considered the time after the smoulder ignited and ambient air was injected to facilitate self-sustained smouldering, i.e., following the typical protocol in smouldering experiments (e.g., [29, 41-43]).

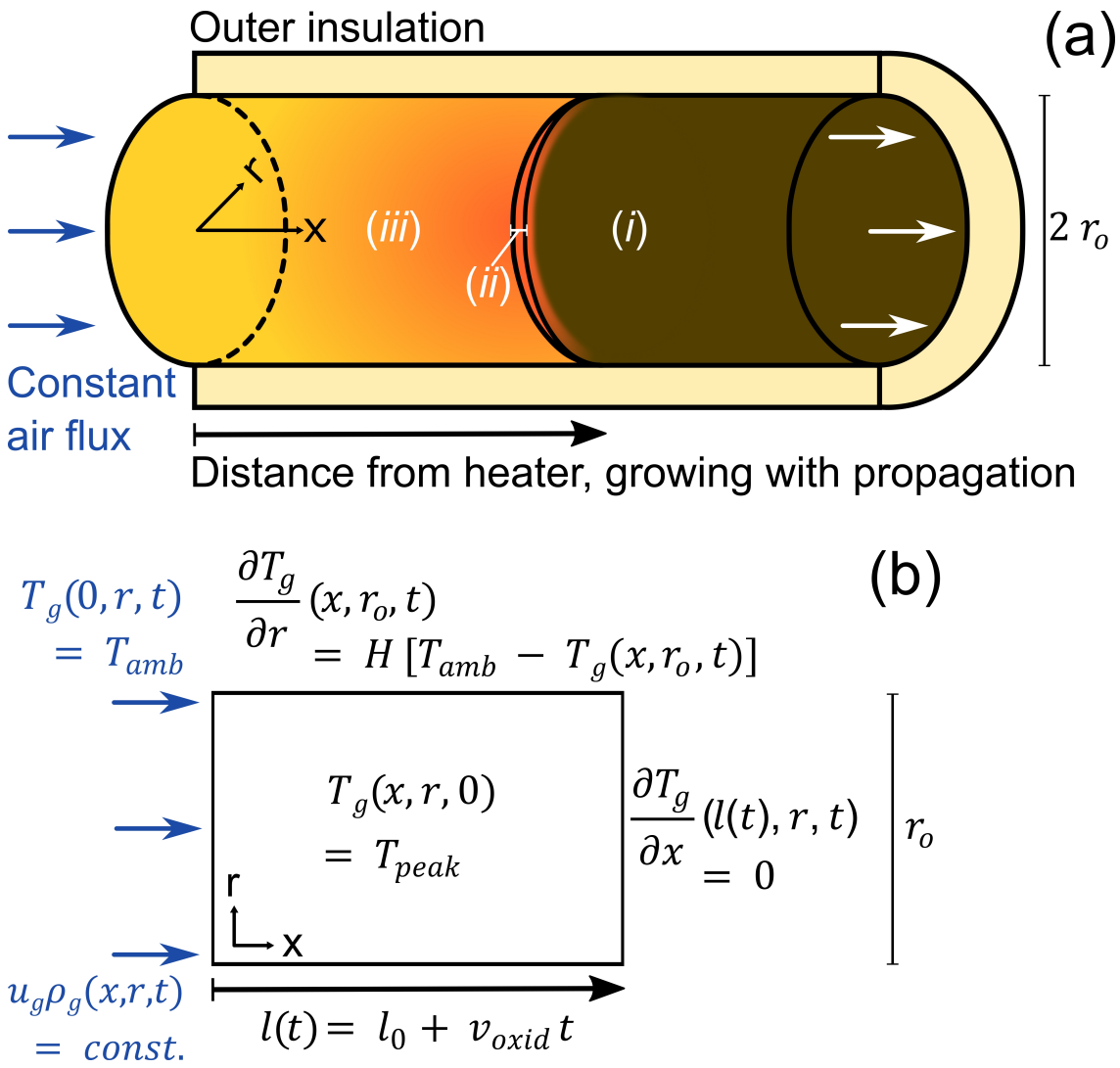

Fig. 2. (a) sketch of the smouldering system where (*i*), (*ii*), and (*iii*) indicate the *Inert Heating Zone*, *Reaction Zone* and *Cooling Zone*, respectively, and (b) extending the conceptual model of a reaction-leading, forward smouldering system from Fig. 1 into a 2-dimensional radial model domain with the boundary and initial conditions from Kuznetsov [38] and with the axial domain length $(l(t))$ expanding with the smoulder velocity (v_{oxid}).

The model domain had an initial length, l_0, i.e., the distance the smouldering front travelled before turning off the heater (as determined by the ignition protocol). This length grew with time as $v_{oxid} > v_{cool}$. Therefore, the analysis of Kuznetsov [38] was extended so that the axial domain length, $l(t)$, grew as the smouldering front propagated, $dl/dt =$

v_{oxid}. Therefore, $l(t)$ was approximated as $l(t) = l_0 + v_{oxid}t$. This expanding domain approximates a moving boundary condition [44], where v_{oxid} was known a priori from experimental observations. Altogether, following Kuznetsov [38], this analysis assumed: (i) LTNE, (ii) incompressible flow, (iii) the air mass flux was uniform across the cross-section and oriented parallel to the length axis, (iv) constant effective thermophysical parameters, (v) the system was axisymmetric, (vi) a convective boundary condition was applied to the outer edge of the column and accounted for the insulation, and (vii) a zero heat flux boundary was applied axially between the cooling and reaction zones (Fig. 1). The porous medium was modelled as a continuum comprised of perfect sand spheres and saturated with air, where the surface porosity was assumed equal to the porosity. The energy equation was modelled in both sand and air phases to allow for heat transfer across phases. Viscous dissipation and work done by pressure changes were neglected, and the effect of radiation was embedded via a diffusive approximation in the solid phase conductivity. These assumptions are further discussed and justified below.

For brevity, only the governing equations, solution, and key distinctions from Kuznetsov [38] are summarized here. The volume-averaged energy equations for the air and sand phases are [38]:

$$\phi\rho_g C_{p_g}\frac{\partial T_g}{\partial t} + \rho_g C_{p_g} u_g \frac{\partial T_g}{\partial x} = \phi k_g\left[\frac{\partial^2 T_g}{\partial x^2} + \frac{\partial^2 T_g}{\partial r^2} + \frac{1}{r}\frac{\partial T_g}{\partial r}\right] + h_{sg}a_{sg}\left(T_s - T_g\right) \quad (2)$$

$$(1-\phi)\rho_s C_{p_s}\frac{\partial T_s}{\partial t} = (1-\phi)k_{s_{app}}\left[\frac{\partial^2 T_s}{\partial x^2} + \frac{\partial^2 T_s}{\partial r^2} + \frac{1}{r}\frac{\partial T_s}{\partial r}\right] - h_{sg}a_{sg}\left(T_s - T_g\right) \quad (3)$$

Radiation heat transfer was embedded in the approximated solid conductivity following the Rosseland approximation, $k_{s_{app}} = k_s + 16\sigma d_p T_s^3/3$ [45], and the specific surface area

was estimated assuming the sand grains were spherical, $a_{sg} = 6(1-\phi)/d_p$ [38, 45]. The heat transfer coefficient between phases, h_{sg}, was approximated following Zanoni et al., [45]. A discussion on the use of Eq. (4) is provided in the Supplementary Materials, Section S2, which is valid for Pr = 0.72, 0.5 ≤ Re ≤ 31, and 0.125 ≤ d_p ≤ 2.000 mm:

$$Nu = h_{sg} d_p / k_g = 0.001\left(Re^{1.97}\mathrm{Pr}^{1/3}\right) \tag{4}$$

The initial condition assumed the air temperature axially and radially across the reactor uniformly reached the peak smouldering temperature [38]:

$$T_g(x, r, 0) = T_{peak} \tag{5}$$

In other words, Eq. (5) assumed the smouldering reactions proceeded with constant intensity both axially and radially as they propagated up the reactor. This is often observed in robust smouldering within inert media (e.g., [42, 43, 46, 47]). Furthermore, near-wall extinction, which is sometimes observed in laboratory experiments as a thin ring of char inside the reactor wall [41, 48], was neglected.

The boundary conditions were defined as [38]:

$$T_g(0, r, t) = T_{amb} \tag{6}$$

$$\frac{\partial T_g}{\partial r}(x, r_o, t) = H\left(T_{amb} - T_g(x, r_o, t)\right) \tag{7}$$

$$\frac{\partial T_g}{\partial x}(l(t), r, t) = 0 \tag{8}$$

Equation (6) assumed ambient temperature air was constantly injected $\left(u_g \rho_g(x, r, t) = const.\right)$ into the reactor. Equation (7) assumed a convective boundary at the edge of the insulation, where the temperature varied steadily across the thickness of the wrapped

insulation (Fig. 2). These assumptions are embedded within the modified effective heat transfer coefficient, i.e., $H = \left(k_{bulk} r_o \left[ln\{r_{o_{ins}}/r_o\}/k_{bulk_{ins}} + 1/h_{ins}\{r_{o_{ins}}\}\right]\right)^{-1}$, where $r_{o_{ins}}$ is the outer radius of the insulation. However, as the heat transfer coefficient at the outer edge of the insulation, h_{ins}, and the effective bulk conductivity of the insulation, $k_{bulk_{ins}}$, were both unknown, H was varied as a bulk parameter in the subsequent analysis.

Equation (8) assumed that the gas temperature did not change axially at the end of the domain. This is reasonable because the interface between the cooling and reaction zones is characterized by a zero temperature gradient (Fig. 1); this assumption is often used in analytical solutions of a travelling smouldering front, e.g., [7, 8, 23, 29]. Importantly, Eq. (8) is only applicable to early, transient system behaviour (i.e., expanding cooling zones); this matches the behaviour of interest as articulated above. See the Supplementary Materials, Section S1, for further discussion on the early versus late time behaviour. The subsequent analysis focused on results that were sufficiently far from the late-time conditions to be relevant to applied smouldering systems.

2.2. Model Solution Method

2.2.1. Descriptions of Dimensionless Parameters

Following the methodology of Kuznetsov [38], a small dimensionless parameter was defined as $\delta = \phi \left(\rho_g C_{p_g}\right)^3 u_g^2 / h_{sg} a_{sg} \left(\rho C_p\right)_{bulk} k_{bulk}$, where $\phi \rho_g C_{p_g} + (1-\phi)\rho_s C_{p_s} = \left(\rho C_p\right)_{bulk}$ and $\phi k_g + (1-\phi) k_{s_{app}} = k_{bulk}$. By balancing bulk energy diffusion and storage with convection, the characteristic length, x_c, and time, t_c, were identified [38]:

$$\left(\rho C_p\right)_{bulk}\frac{\Delta T}{t_c} \sim \rho_g C_{p_g} u_g \frac{\Delta T}{x_c} \sim k_{bulk}\frac{\Delta T}{x_c^2} \tag{9}$$

Equation (9) implies $x_c = k_{bulk}/\rho_g C_{p_g} u_g$ and $t_c = \left(\rho C_p\right)_{bulk} k_{bulk}/\left(\rho_g C_{p_g} u_g\right)^2$, and the dimensionless distances and times were defined as $\xi_x = x/x_c$, $\xi_r = r/x_c$, and $\tau = t/t_c$ [38]. Dividing the characteristic distance by time leads to the cooling velocity: $v_{cool} = \rho_g C_{p_g} u_g/\left(\rho C_p\right)_{bulk}$ [35, 38]. The dimensionless temperature was defined as $\theta = (T - T_{peak})/(T_{amb} - T_{peak})$, where the degree of LTNE was assumed small and treated as $\theta_s = \theta_g + \delta\Delta\theta$ [38].

2.2.2. Summary of Key Analytical Solutions

The solution to Eqs. (2-3) was obtained following the method of Kuznetsov [38], essentially by separating the axial convective-diffusive and radial diffusive equations and combining their solutions together. The non-dimensional forms of Eqs. (2-3) and key intermediate steps are included in the Supplementary Materials, Section S3. The solution for the dimensionless air temperature is [38]:

$$\theta_g(\xi_x, \xi_r, \tau) = 1 - \sum_{n,m=1}^{\infty} c_n \exp\left(\frac{\xi_x}{2} - \left[\frac{1}{4} + b_n^2 + \frac{\gamma_m^2}{R^2}\right]\tau\right)\frac{2\alpha R sin(b_n\xi_x) J_0\left(\frac{\xi_r\gamma_m}{R}\right)}{(\gamma_m^2 + \alpha^2 R^2) J_0(\gamma_m)} \tag{10}$$

where $c_n = (1/4 + b_n^2)^{-1} \times [L/2b_n - \sin(2b_n L)/4b_n^2]^{-1}$, and b_n and γ_m are the positive roots from the transcendental equations $tan(b_n L) = -2b_n$ and $J_1(\gamma_m) = \alpha R J_0(\gamma_m)$, respectively. The difference between phase temperature was then solved as [38]:

$$\Delta\theta(\xi_x, \xi_r, \tau)$$

$$= -\sum_{n,m=1}^{\infty} \frac{2\alpha R c_n \exp\left(\frac{\xi_x}{2} - \left[\frac{1}{4} + b_n^2 + \frac{\gamma_m^2}{R^2}\right]\tau\right) J_0\left(\frac{\xi_r \gamma_m}{R}\right)}{(\gamma_m^2 + \alpha^2 R^2) J_0(\gamma_m)} \times \left\{ \begin{array}{c} sin(b_n \xi_x)\left[-\frac{1}{4} - b_n^2 - \frac{\gamma_m^2}{R^2} + \frac{\Lambda_1}{2} - \frac{\Lambda_2}{4} + \Lambda_2 b_n^2 + \Lambda_2\left(\frac{\gamma_m}{R}\right)^2\right] \\ +cos(b_n \xi_x) b_n [\Lambda_1 - \Lambda_2] \end{array} \right\} \quad (11)$$

where $\Lambda_1 = \left(\rho C_p\right)_{bulk} / \phi \rho_g C_{p_g}$, $\Lambda_2 = k_g \left(\rho C_p\right)_{bulk} / \rho_g C_{p_g} k_{bulk}$, $R = r_0 / x_c$, $L(\tau) = l(t)/x_c$, and $\alpha = H x_c$.

2.2.3. Details on Model Input Parameters

To solve Eqs. (10-11), values from smouldering experiments averaged just after ignition were used: T_{peak} = 862°C and v_{oxid} = 0.44 cm min^{-1} [33]. These experiments were performed in reactors with 0.08 m and 0.30 m radii, respectively, using granular activated carbon (the fuel) in sand (the IPM) at a fuel/sand mass ratio of 23.3 g_{fuel} kg_s^{-1} and with a forced Darcy air flux of 0.050 m s^{-1} at standard temperature and pressure (i.e., a constant mass flux of 0.060 kg m^{-2} s^{-1}). These experiments had specific experimental errors associated with the setups, which are summarized in the Supplementary Materials, Table S1. Additional details of these experiments can be found in [33, 49, 50]. These smouldering experiments showed comparable T_{peak} and v_{oxid} at both scales, which is consistent with Switzer et al., [34]. Moreover, the peak temperature and propagation velocity used here compare well with other smouldering experiments with similar fuel concentrations in sand (e.g., [32, 43]).

The l_0 was set to 0.13 mand the temperature-dependant effective thermophysical parameters were estimated over T_{amb} to T_{peak}, e.g., $\rho C_{p_{eff}} = \int_{T_{amb}}^{T_{peak}} \rho C_p(T) dT \,/ \left(T_{peak} -\right.$

T_{amb}). See Table 1 for all parameters and references [33, 45, 49] for thorough descriptions of the parameter errors.

Table 1.
Model Input Parameters.

Par.	Value	Unit	Ref.
T_{peak}	862	°C	[33]
T_{amb}	21	°C	[33]
$\rho_g u_g$	0.060	kg m^{-2} s^{-1}	[33]
v_{oxid}	7.3×10^{-5}	m s^{-1}	[33]
l_0	0.13	m	[33]
ϕ	0.37	-	[45]
d_p	2.00×10^{-3}	m	[45]
ρ_s	2650	kg m^{-3}	[45]
σ	5.67×10^{-8}	W m^{-2} K^{-4}	[45]
C_{p_s}	1591	J kg^{-1} K^{-1}	[45]
C_{p_g}	1085	J kg^{-1} K^{-1}	[45]
μ	2.95×10^{-5}	Pa s	[45]
$k_{s_{app}}$	0.844	W m^{-1} K^{-1}	[45]
k_g	5.58×10^{-2}	W m^{-1} K^{-1}	[45]

2.2.4. Solving Eqs. (10-11)

All calculations of Eqs. (10-11) used 60 roots to minimize solution instabilities in $\theta_g(\xi_x, \xi_r, \tau)$ near $\xi_x = L(\tau)$. However, Eqs. (10-11) have a few limitations. Because of the thermal shock at $(\xi_x, \xi_r, \tau) = (0, \xi_r, 0)$, Eqs. (10-11) cannot estimate the temperature

difference between phases near $\tau = 0$ [35, 36, 38]. Also, because in this analysis $v_{oxid} > v_{cool}$, instabilities will appear at $\theta_g(\xi_x, \xi_r, \tau)$ near $\xi_x = L(\tau)$. This is because Eq. (10) becomes unstable near $\xi_x = L$ at large values of L/τ. Here, $L(\tau)$ constantly increased, and the solution became more unstable over time near $\xi_x = L$ because $dL(\tau)/d\tau = v_{oxid}/v_{cool}$ =2.9. These two limitations were avoided by focusing on the cooling behaviour between 25 and 45 minutes, when the smouldering front travelled from 0.24 to 0.33 m, respectively, which was identified heuristically. Moreover, as Eq. (8) is not appropriate near steady-state conditions at late times in relatively long reactors, a simple criterion to identify late-time conditions (which is a function of system properties, e.g., radius and insulation) was estimated (see Supplementary Materials, Section S4). This criterion shows that estimates from reactors with radii > $O(0.1)$ m are sufficiently far from the late-time conditions within the chosen timeframe. That is, the model as applied here is appropriate for analyzing laboratory scale and commercial scale reactors. Though applications of the model to very small reactors with radii ≤ $O(0.01)$ m have greater error due to an incomplete description of the problem, they are qualitatively valuable in illustrating key trends.

2.3. Quantifying Heat Losses

The heat losses were quantified from a simplified global energy balance around the reactor using the dominant terms from Eq. (1) [32]:

$$\dot{E}_{net} = \dot{E}_{oxid} - \dot{E}_{loss} \tag{12}$$

As described above, the net energy is almost entirely in the hot sand $(1-\phi)\rho_s C_{p_s} \gg \phi C_{p_g}\rho_g$. The net stored energy integrated up to a specific time, $E_{net}(t_f)$, was defined as [33]:

$$E_{net}(t_f) = \int_{t_0}^{t_f} (\dot{E}_{net})dt = \iiint_V \int_{T_{amb}}^{T_s(x,r,t_f)} (1-\phi)\rho_s C_{p_s}(T_s)dTdV \quad (13)$$

Here, $t_0 \leq t \leq t_f$ is the cooling duration to define the net stored energy at $t = t_f$ and t_0 is the start of cooling (i.e., assuming heat losses are negligible during ignition [28, 32, 33]). Details on the methods used to integrate Eq. (13), which assumed the temperature distribution was axisymmetric, are included in the Supplementary Materials, Section S5.

Equation (13) calculates $E_{net}(t_f)$ with heat losses drawing energy out of the reactor. To contrast against a case without heat losses, $E_{net,adiabatic}(t_f)$ was estimated by resolving Eqs. (10-11,13) with α =0.0001, so $O(\alpha) = O(\delta)$. Using a small α effectively simulated a very well insulated reactor so that $T_s(x,t)$ no longer varied along the reactor radius. The comparison between these two cases was expressed as the system energy efficiency [33]:

$$System\ Energy\ Efficiency = E_{net}(t)/E_{net,adiabatic}(t) \sim [E_{oxid}(t) - E_{loss}(t)]/E_{oxid}(t) \quad (14)$$

3. Results and Discussion

Figure 3 shows the modelled centreline temperatures in both the solid and gas phases, $T_s(x)$ and $T_g(x)$, in the small (0.08 m radius) and large (0.30 m radius) reactors at the bounding times i.e., after 25 and 45 minutes. The analysis used all values in Table 1, unless otherwise noted. Figure 3 shows the predicted degree of LTNE, which was highest along the centreline of the reactor as also observed by Kuznetsov [38]. Here, the maximum predicted difference between phase temperatures was 16% and 14% of $T_{peak} - T_{amb}$ after 25 and 45 minutes, respectively. This confirms that the degree of LTNE was relatively small in the cooling zone and therefore appropriate for the perturbation technique used. Furthermore, Fig. 3 shows the velocity of the cooling front (0.15 cm min^{-1}) is predicted to be independent of radius.

Figure 3 also shows the centreline temperatures just behind the smouldering front, near $x = l(t)$, slightly decreasing with time because of radial heat losses. Figure 3(a) shows the peak temperature in the small reactor drops from 859°C to 820°C from 25 minutes to 45 minutes, respectively, and Figure 3(b) shows a smaller drop in the large reactor from 862°C to 859°C over the same period. This aligns with experimental observations, as heat losses can lower subsequent centreline peak temperatures, e.g., observed in [29]. In limiting cases, high heat losses can lower smouldering temperatures to the point of extinction [1, 4, 23, 28, 49]. In line with the numerical observations from [28], it is postulated here that heat losses in the cooling zone (upstream of reactions, Fig. 1) may be responsible for these effects on the reaction characteristics. Importantly, as the reactor radius increases the centreline temperatures are less sensitive to radial heat losses, as expected [4].

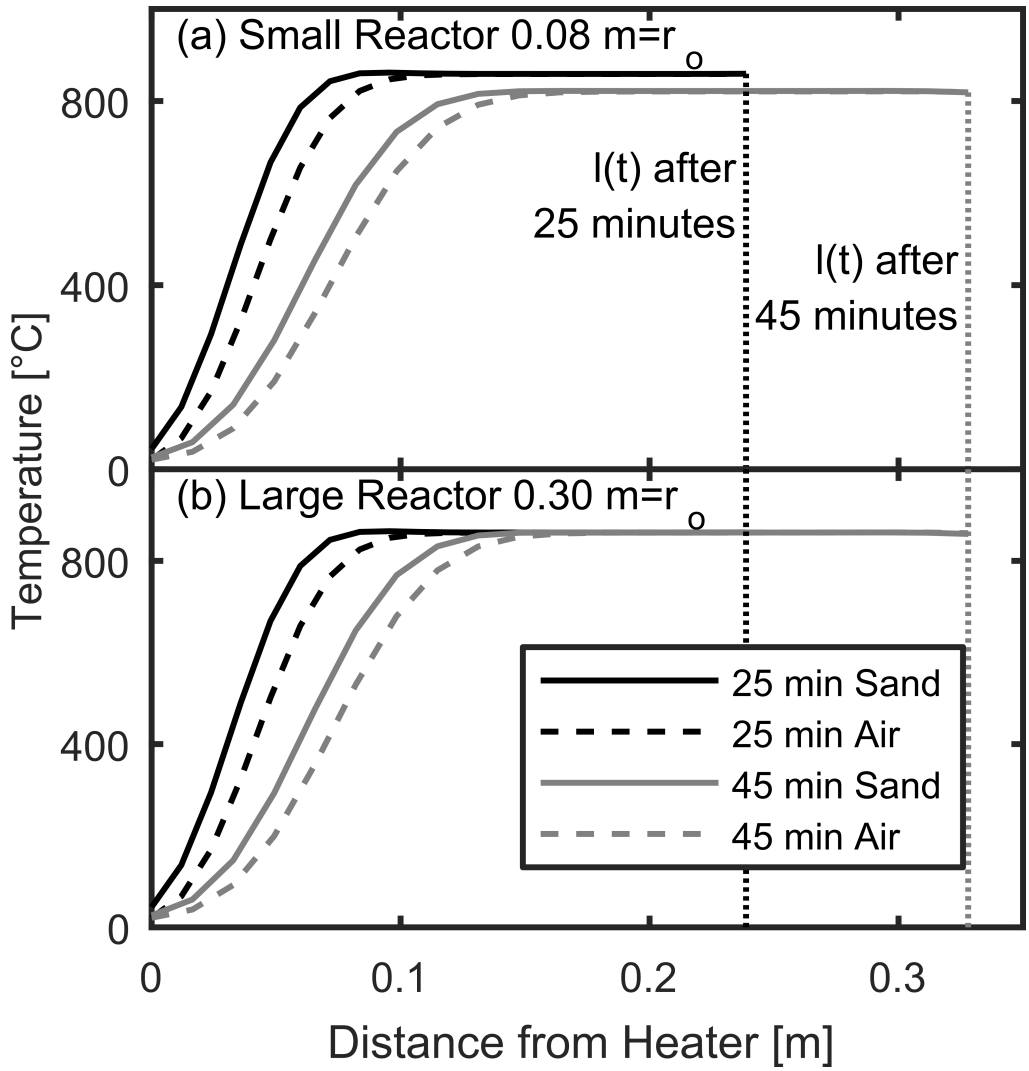

Fig. 3. Sand and air temperatures along the centreline in the cooling zone after 25 minutes and 45 minutes in the (a) small and (b) large reactors.

Figure 4 visualizes the modelled sand temperature profile throughout the radial and axial coordinates in the cooling zone when the smouldering front travelled 0.33 m after 45 minutes. Figure 4 captures the general spatial features in temperatures reported from other applied smouldering studies [29-31]. For example, though the centreline peak temperatures are relatively close to the observed peak smouldering temperature (862°C), the peak temperatures decrease with radius, particularly within 0.1 m of the wall (i.e., near

$r = r_o$). These locations near reactor walls are most sensitive to radial heat losses, therefore cooler peak temperatures near reactor walls are consistently observed in smouldering studies with radial temperature measurements [29-31, 33, 46]. The differences in the temperature profiles between the small and large reactors match expectations. Like in Fig. 3, here it is hypothesized that heat losses in the cooling zone may be responsible for these cooler peak temperatures near the walls. Overall, Figures 2 and 3 provide confidence in the performance of the model and suggest its versatility and value for further analysis, such as exploring energy efficiency.

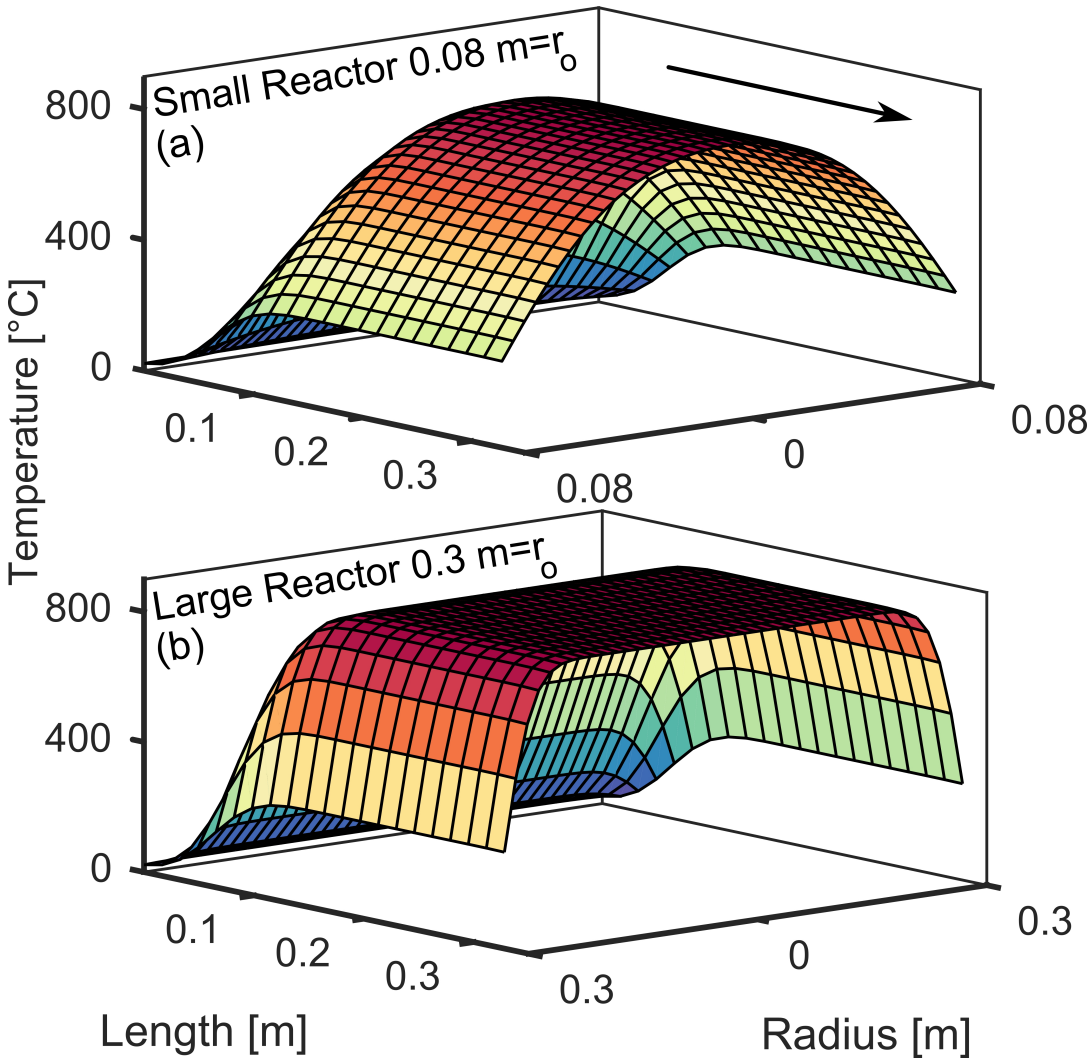

Fig. 4. Sand temperatures in the cooling zone when the smouldering front travelled 0.33 m after 45 minutes of cooling in the small (a) and large (b) reactor. The arrow indicates the direction of smouldering propagation in both (a) and (b).

By integrating over the temperature profiles using Eq. (13), the total heat losses were estimated. Figure 5 quantifies the role of radial heat losses on the system energy efficiency (Eq. (14)) in simulated reactors with radii from 0.002 to 0.5 m and varying degrees of insulation (α). For simplicity, all calculations in Fig. 5 estimate the system energy efficiency at just one time (45 minutes). Note that the experimental and numerical data points plotted in Fig. 5 are all within the envelope of valid, early-time conditions for

applying the model (see Fig. S4 and related discussion in the Supplementary Materials, Section S4). Note also that the shaded region in Fig. 5 marks the approximate region, as the radii approaches $O(0.01)$ m, where the early-time assumptions are less valid and the results should be considered only qualitative (see additional discussion in the Supplementary Materials, Sections S1 and S4).

The model solution (lines) plotted in Fig. 5 illustrate how the role of heat losses diminishes significantly, and thus system energy efficiency increases rapidly, as reactor radius increases. This is due to decreasing surface-area-to-volume ratio ($2/r$). Below a radius of 0.1 m (the size of most laboratory smouldering systems), the system is highly sensitive to heat losses and insulation quality. At this radius, system energy efficiency is bounded between 57% and 86%, with a practical value (α = 0.5) of approximately 64%. This sensitivity attenuates up to a radius of ~0.4 m, beyond which the model predicts the system is relatively insensitive to reactor radius or insulation quality. At this radius, system energy efficiency is bounded between 87% and 96%, with a practical value of approximately 90%. These relationships suggest that batch reactors designed for applied smouldering do not need to exceed approximately 0.4 m in radius and can ignore insulation to protect against heat losses.

Moreover, Fig. 5 implies how the reactor radius affects the smouldering propagation limits in these systems. Though extinction is not explicitly considered in this analysis, regions near the walls in small radius reactors with relatively poor insulation (i.e., high α) suffer most from radial heat losses. As shown in Fig. 4, peak temperatures drop near the reactor walls due to heat losses in the cooling zone and, if severe, may lead to extinction. In limiting cases, this extinction region near the reactor walls would grow into the reactor

centre as the smouldering front propagates and lead to non-self-sustaining smouldering, e.g., observed as conical burn shapes profiles in polyurethane foam [1, 23] or as diminishing centreline temperatures [28, 32, 42, 47]. If the insulation quality is kept fixed in these limiting cases, a minimum reactor radius is required to overcome radial heat losses [1, 4].

Additional insight into the system energy efficiency evolution throughout propagation and an alternative interpretation of the heat losses estimated in Fig. 5 are provided in the Supplementary Materials (Figs. S4 and S5, respectively). These figures are provided to help clarify the transient nature of the system energy efficiency and to support the key comparisons made in Fig. 5.

Overall, Fig. 5 shows an envelope of calculations, bounded by assumptions on the insulation quality, which captures the complexity of available published data. As Zanoni et al., [28] showed, the role of heat losses in a smouldering system results from a complicated interplay between many factors affecting the global energy balance in Eq. (1). Therefore, the system energy efficiencies from disjointed studies are not expected to collapse onto a single curve in Fig. 5, but instead scatter due to their specific experimental/numerical conditions. These studies investigated applied smouldering under a range of conditions, e.g., varying Darcy air fluxes, porous media type, fuel type and fuel concentration (see further details on these studies in the Supplementary Materials, Section S4). As an exception, the estimates in [33] do line up well near the $\alpha = 0.5$ curve, as they mirrored the conditions considered in this analysis (the details on this insulation used in [33] are provided in the Supplementary Materials, Section S4). These experiments are therefore the best comparison for Fig. 5 and, because they show

excellent agreement with the key trends in Fig. 5, matching predictions at both (0.08 m, 56%) and (0.30 m, 87%), they provide confidence that the main physics governing heat losses across scales are captured in this analysis. Therefore, Fig. 5 shows that heat losses from a smouldering system are governed by heat diffusion from the cooling zone, and their impact on the global energy balance attenuates as expected with the additional heat diffusion resistance as the reactor radius increases and insulation improves.

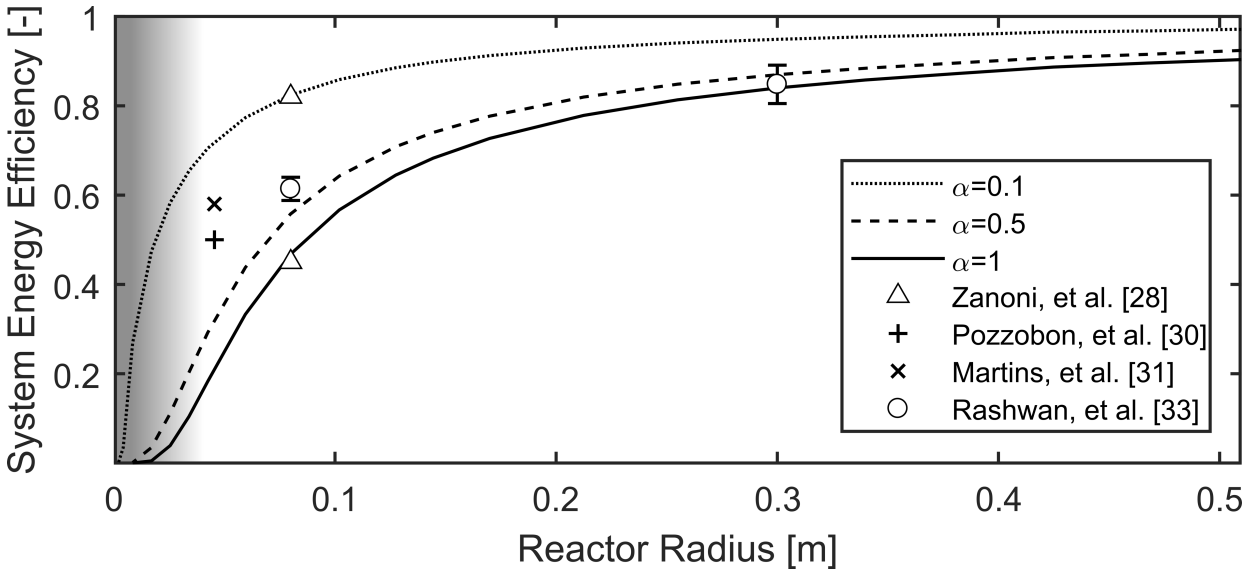

Fig. 5. System energy efficiencies estimated when the smouldering front travelled 0.33 m after 45 minutes of cooling in reactors with varying radii and assuming insulation was relatively poor ($\alpha = 1$), good ($\alpha = 0.5$), and very good ($\alpha = 0.1$). Experimental and numerical observations from similar studies are plotted for comparison. The error bars on experimental values represent the median absolute deviations of estimates. The gradient gray area approximately shows the region where the assumptions regarding the boundary condition in Eq. (8) becomes less valid as the radius decreases to O(0.01 m).

4. Conclusions

As smouldering-based systems gain popularity for a variety of energy conversion purposes, there is a strong interest in optimizing the reactor design to support robust smouldering. Heat losses play a critical role in the energy balance of these smouldering systems, and therefore have strong implications on understanding propagation limits and reactor design. In this work, the increased energy efficiency with reactor radius was modelled via a global energy balance. This represents the first attempt to quantitatively plot the improved energy efficiency with scale in applied smouldering systems. By repurposing the analytical solution from Kuznetsov [38], with the domain length growing with a known smouldering velocity, the radial heat losses behind a forward smouldering front were approximated and expressed as a system energy efficiency. This analysis was completed on simulated reactors with 0.002 to 0.5 m radii and the results compare well with existing experimental and numerical estimates of heat losses from similar smouldering systems. The system energy efficiency was shown to increase in reactors with improved insulation and to dramatically increase with increased radius up to ~0.1 m in radius (i.e., laboratory-sized reactors), and improve more gradually up to ~0.4 m in radius. However, beyond 0.4 m, the system energy efficiency was relatively insensitive to increases in reactor radius and insulation quality. These results are highly relevant for commercial smouldering systems in batch operation, which are currently being used to manage stockpiles of hazardous wastes [9-11, 19] and suggests that these smouldering systems do not need to be much larger than 0.4 m in radius to protect against heat losses. This should allow for reduced reactor costs and allow for optimization with respect to energy efficiency and energy recovery.

5. Acknowledgements

Funding was provided by the Ontario Ministry of Research, Innovation, and Science; the Government of Canada through the Federal Economic Development Agency for Southern Ontario through the Southern Ontario Water Consortium's Advancing Water Technologies Program (Grant SUB02392) with in-kind support from: 1) the Ontario Ministry of the Environment, Conservation and Parks and 2) Savron (a wholly owned subdivision of Geosyntec Consultants Ltd); the Water Environment Association of Ontario's Residuals and Biosolids Research Fund Award (2018 and 2019); and the Natural Sciences and Engineering Research Council of Canada (Graduate Scholarship PGSD3 - 489978 - 2016 and Grant Nos. CREATE 449311-14, RGPIN 2018-06464 and RGPAS-2018-522602). Additional project support from Gudgeon Thermfire International, especially from Justin Barfett and Randy Adamski, and a travel stipend to the first author from the Remediation Education Network (RENEW) Program are also gratefully acknowledged.

6. References

[1] G. Rein, Smoldering Combustion, in: M.J. Hurley, D.T. Gottuk, J.R. Hall Jr, K. Harada, E.D. Kuligowski, M. Puchovsky, J.L. Torero, J.M. Watts Jr, C.J. Wieczorek (Eds.) SFPE Handbook of Fire Protection Engineering, Springer New York, New York, NY, 2016, pp. 581-603.
[2] B. Shi, H. Su, J. Li, H. Qi, F. Zhou, J.L. Torero, Z. Chen, Clean Power Generation from the Intractable Natural Coalfield Fires: Turn Harm into Benefit, Sci. Rep., 7(1) (2017) 5302.
[3] H. Chen, G. Rein, N. Liu, Numerical investigation of downward smoldering combustion in an organic soil column, Int. J. Heat Mass Transfer, 84 (2015) 253-261.
[4] S. Lin, X. Huang, Quenching of smoldering: Effect of wall cooling on extinction, Proc. Combust. Inst., (2020) https://doi.org/10.1016/j.proci.2020.1005.1017.
[5] S.V. Glazov, V.M. Kislov, E.A. Salgansky, O.S. Rabinovich, A.I. Malinouski, M.V. Salganskaya, E.N. Pilipenko, Y.Y. Kolesnikova, Effect of local rearrangements in the particle bed on the stability of filtration combustion of solid fuel, Int. J. Heat Mass Transfer, 108 (2017) 1602-1609.
[6] G.B. Manelis, S.V. Glazov, E.A. Salgansky, D.B. Lempert, I.Y. Gudkova, I.A. Domashnev, A.M. Kolesnikova, V.M. Kislov, Y.Y. Kolesnikova, Extraction of molybdenum-containing species from heavy oil residues using the filtration combustion method, Int. J. Heat Mass Transfer, 92 (2016) 744-750.
[7] J. Bruining, A.A. Mailybaev, D. Marchesin, Filtration Combustion in Wet Porous Medium, SIAM Journal on Applied Mathematics, 70(4) (2009) 1157-1177.
[8] A.P. Aldushin, I.E. Rumanov, B.J. Matkowsky, Maximal energy accumulation in a superadiabatic filtration combustion wave, Combust. Flame, 118(1–2) (1999) 76-90.
[9] G. Sabadell, D. Thomas, P. Bireta, G. Scholes, C. Murray, B. Boulay, G. Grant, D. Major, Treatment of Oil-Impacted Soil and Oily Waste: Overview of Two Field Demonstration Projects, in: SPE International Conference and Exhibition on Health, Safety, Security, Environment, and Social Responsibility, Society of Petroleum Engineers, Abu Dhabi, UAE, 2018, pp. SPE-190566-MS.
[10] G. Sabadell, G. Scholes, D. Thomas, C. Murray, P. Bireta, G. Grant, D. Major, Ex situ treatment of organic wastes or oil-impacted soil using a smoldering process, WIT Trans. Ecol. Environ., 231 (2019) 367-376.
[11] D. Thomas, P. Bireta, K. McVey, D. Segal, M. Hudson, B.-H. Sami, S. Gabriel, A Novel, Cost Effective and Easily Scaled Solution for On-Site Treatment of Oily Wastes, in: International Petroleum Technology Conference, International Petroleum Technology Conference, Dhahran, Kingdom of Saudi Arabia, 2020, pp. IPTC-19951-MS.
[12] G.P. Grant, D. Major, G.C. Scholes, J. Horst, S. Hill, M.R. Klemmer, J.N. Couch, Smoldering Combustion (STAR) for the Treatment of Contaminated Soils: Examining Limitations and Defining Success, Rem. J., 26(3) (2016) 27-51.
[13] J.E. Vidonish, K. Zygourakis, C.A. Masiello, G. Sabadell, P.J.J. Alvarez, Thermal Treatment of Hydrocarbon-Impacted Soils: A Review of Technology Innovation for Sustainable Remediation, Engineering, 2(4) (2016) 426-437.
[14] G. Gianfelice, M. Della Zassa, A. Biasin, P. Canu, Onset and propagation of smouldering in pine bark controlled by addition of inert solids, Renew. Energ., 132 (2019) 596-614.

[15] H.K. Wyn, M. Konarova, J. Beltramini, G. Perkins, L. Yermán, Self-sustaining smouldering combustion of waste: A review on applications, key parameters and potential resource recovery, Fuel Process. Technol., 205 (2020) 106425.
[16] A. Serrano, H. Wyn, L. Dupont, D.K. Villa-Gomez, L. Yermán, Self-sustaining treatment as a novel alternative for the stabilization of anaerobic digestate, J. Environ. Manage., 264 (2020) 110544.
[17] J.-P. Vantelon, B. Lodeho, S. Pignoux, J.L. Ellzey, J.L. Torero, Experimental observations on the thermal degradation of a porous bed of tires, Proc. Combust. Inst., 30(2) (2005) 2239-2246.
[18] S. Saberi, K. Samiei, E. Iwanek, S. Vohra, M. Farkhondehkavaki, Y.-L. Cheng, Treatment of fecal matter by smoldering and catalytic oxidation, J Water Sanit Hyg Dev, 10(2) (2020) 219–226.
[19] R. Solinger, G.P. Grant, G.C. Scholes, C. Murray, J.I. Gerhard, STARx Hottpad for smoldering treatment of waste oil sludge: Proof of concept and sensitivity to key design parameters, Waste Manage. Res., 38(5) (2020) 554-566.
[20] J.I. Gerhard, G.P. Grant, J.L. Torero, Chapter 9 - Star: a uniquely sustainable in situ and ex situ remediation process, in: D. Hou (Ed.) Sustainable Remediation of Contaminated Soil and Groundwater, Butterworth-Heinemann, 2020, pp. 221-246.
[21] T.J. Ohlemiller, Modeling of smoldering combustion propagation, Prog. Energ. Combust., 11(4) (1985) 277-310.
[22] F.A. Williams, Combustion theory, second ed., Addison-Wesley Publishing Company, Menlo Park, California, 1985.
[23] J.L. Torero, J.I. Gerhard, M.F. Martins, M.A.B. Zanoni, T.L. Rashwan, J.K. Brown, Processes defining smouldering combustion: Integrated review and synthesis, Prog. Energ. Combust., 81 (2020) 100869.
[24] N.A. Moussa, T.Y. Toong, C.A. Garris, Mechanism of smoldering of cellulosic materials, Symp. (Int.) Combust., 16(1) (1977) 1447-1457.
[25] M.A.B. Zanoni, G. Rein, L. Yermán, J.I. Gerhard, Thermal and oxidative decomposition of bitumen at the Microscale: Kinetic inverse modelling, Fuel, 264 (2020) 116704.
[26] F.A. Williams, Mechanisms of fire spread, Symp. (Int.) Combust., 16(1) (1977) 1281-1294.
[27] G.C. Scholes, J.I. Gerhard, G.P. Grant, D.W. Major, J.E. Vidumsky, C. Switzer, J.L. Torero, Smoldering Remediation of Coal-Tar-Contaminated Soil: Pilot Field Tests of STAR, Environ. Sci. Technol., 49(24) (2015) 14334-14342.
[28] M.A.B. Zanoni, J.L. Torero, J.I. Gerhard, Delineating and explaining the limits of self-sustained smouldering combustion, Combust. Flame, 201 (2019) 78-92.
[29] G. Baud, S. Salvador, G. Debenest, J.-F. Thovert, New Granular Model Medium To Investigate Smoldering Fronts Propagation—Experiments, Energ. Fuel., 29(10) (2015) 6780-6792.
[30] V. Pozzobon, G. Baud, S. Salvador, G. Debenest, Darcy Scale Modeling of Smoldering: Impact of Heat Loss, Combust. Sci. Technol., 189(2) (2017) 340-365.
[31] M.F. Martins, S. Salvador, J.F. Thovert, G. Debenest, Co-current combustion of oil shale – Part 2: Structure of the combustion front, Fuel, 89(1) (2010) 133-143.

[32] M.A.B. Zanoni, J.L. Torero, J.I. Gerhard, Determining the conditions that lead to self-sustained smouldering combustion by means of numerical modelling, Proc. Combust. Inst., 37(3) (2019) 4043-4051.
[33] T.L. Rashwan, J.L. Torero, J.I. Gerhard, The improved energy efficiency of applied smouldering systems with increasing scale, (submitted).
[34] C. Switzer, P. Pironi, J.I. Gerhard, G. Rein, J.L. Torero, Volumetric scale-up of smouldering remediation of contaminated materials, J. Hazard. Mater., 268 (2014) 51-60.
[35] A.V. Kuznetsov, An investigation of a wave of temperature difference between solid and fluid phases in a porous packed bed, Int. J. Heat Mass Transfer, 37(18) (1994) 3030-3033.
[36] A.V. Kuznetsov, THERMAL NONEQUILIBRIUM FORCED CONVECTION IN POROUS MEDIA, in: D.B. Ingham, I. Pop (Eds.) Transport Phenomena in Porous Media, Pergamon, Oxford, 1998, pp. 103-129.
[37] T.E.W. Schumann, Heat transfer: A liquid flowing through a porous prism, J. Frankl. Inst., 208(3) (1929) 405-416.
[38] A.V. Kuznetsov, Investigation of a Non-Thermal Equilibrium Flow of an Incompressible Fluid in a Cylindrical Tube Filled with Porous Media, ZAMM-Z. Angew. Math. Me., 76(7) (1996) 411-418.
[39] S. Kuravi, J. Trahan, D.Y. Goswami, M.M. Rahman, E.K. Stefanakos, Thermal energy storage technologies and systems for concentrating solar power plants, Prog. Energ. Combust., 39(4) (2013) 285-319.
[40] P. Basu, Biomass gasification and pyrolysis: practical design and theory, Academic Press, Oxford, 2010.
[41] P. Pironi, C. Switzer, G. Rein, A. Fuentes, J.I. Gerhard, J.L. Torero, Small-scale forward smouldering experiments for remediation of coal tar in inert media, Proc. Combust. Inst., 32(2) (2009) 1957-1964.
[42] T.L. Rashwan, J.I. Gerhard, G.P. Grant, Application of self-sustaining smouldering combustion for the destruction of wastewater biosolids, Waste Manage., 50 (2016) 201-212.
[43] M.A.B. Zanoni, J.L. Torero, J.I. Gerhard, The role of local thermal non-equilibrium in modelling smouldering combustion of organic liquids, Proc. Combust. Inst., 37(3) (2019) 3109-3117.
[44] J. Crank, Free and Moving Boundary Problems, Clarendon Press, Oxford, 1987.
[45] M.A.B. Zanoni, J.L. Torero, J.I. Gerhard, Determination of the interfacial heat transfer coefficient between forced air and sand at Reynold's numbers relevant to smouldering combustion, Int. J. Heat Mass Transfer, 114(Supplement C) (2017) 90-104.
[46] I. Fabris, D. Cormier, J.I. Gerhard, T. Bartczak, M. Kortschot, J.L. Torero, Y.-L. Cheng, Continuous, self-sustaining smouldering destruction of simulated faeces, Fuel, 190 (2017) 58-66.
[47] L. Yermán, R.M. Hadden, J. Carrascal, I. Fabris, D. Cormier, J.L. Torero, J.I. Gerhard, M. Krajcovic, P. Pironi, Y.-L. Cheng, Smouldering combustion as a treatment technology for faeces: Exploring the parameter space, Fuel, 147 (2015) 108-116.
[48] M.A.B. Zanoni, J.L. Torero, J.I. Gerhard, Experimental and numerical investigation of weak, self-sustained conditions in engineered smouldering combustion, Combust. Flame, 222 (2020) 27-35.

[49] T.L. Rashwan, Sustainable Smouldering for Waste-to-Energy: Scale, Heat Losses, and Energy Efficiency, PhD, The University of Western Ontario, London, Canada, 2020.
[50] T.L. Rashwan, J.L. Torero, J.I. Gerhard, Heat losses in a smouldering system: The key role of non-uniform air flux, Combust. Flame, 227 (2021) 309-321.